Available online at www.sciencedirect.com
ScienceDirect
Computerized Medical Imaging and Graphics 32 (2008) 554–565
Computerized Medical Imaging and Graphics
www.elsevier.com/locate/compmedimag

An affine transformation invariance approach to cell tracking

Jing Cui [a,*], Nilanjan Ray [b,1], Scott T. Acton [c,2], Zongli Lin [c,3]

[a] Department of Radiology, University of Michigan, Med-Inn C473, 1500 E. Medical Center Drive, Ann Arbor, MI 48109-5842, United States
[b] Department of Computing Science, 2-21 Athabasca Hall, University of Alberta, Edmonton, Alberta, Canada T6G 2E8
[c] Charles L. Brown Department of Electrical and Computer Engineering, Thornton Hall, University of Virginia, 351 McCormick Road, P.O. Box 400743, Charlottesville, VA 22904-4743, United States

Received 16 August 2007; received in revised form 17 June 2008; accepted 19 June 2008

Abstract

Accurate and robust methods for automatically tracking rolling leukocytes facilitate inflammation research as leukocyte motion is a primary indicator of inflammatory response in the microvasculature. This paper reports on an affine transformation invariance approach we proposed to track rolling leukocyte in intravital microscopy image sequences. The method is based on the affine transformation invariance property, which enables the accommodation of linear affine transformations (translation, rotation, and/or scaling) of the target, and a particle filter that overcomes the effect of image clutter. In our data set of 50 sequences, we compared the new approach with an active contour tracking method and a Monte Carlo tracker. With the manual tracking result provided by an operator as the reference, the root mean square errors for the active contour tracking method, the Monte Carlo tracker and the affine transformation invariance approach were 0.95 μm, 0.79 μm and 0.74 μm, respectively, and the percentage of frames tracked were 72%, 75% and 89%, respectively. The affine transformation invariance approach demonstrated more robust (being able to successfully locate target leukocyte in more frames) and more accurate (lower root mean square error) tracking performance. We also separately studied the ability of the affine transformation invariance approach to track a dark target leukocyte and a bright target leukocyte by using the number of frames tracked as an evaluation measure. Dark target leukocyte possesses similar image intensity to the background, making it difficult to be located. In 20 sequences where the target leukocyte was dark, the affine transformation invariance approach tracked more frames in 18 sequences and fewer frames in 2 sequences when compared with the active contour tracking method. In comparison with the Monte Carlo tracker, the affine invariance method tracked more frames in 9 sequences, the same number of frames in 7 sequences and fewer frames in 4 sequences. In tracking a bright target leukocyte in 30 sequences, the affine transformation invariance approach demonstrated superior performance in 7 sequences and inferior performance in 1 sequence when compared with the active contour tracking method. It outperformed the Monte Carlo tracker in 15 sequences and underperformed in 1 sequence.

Keywords: Linear affine transformation; Cell tracking; Particle filter; In vivo; Leukocyte rolling velocity

1. Introduction

Leukocyte rolling behavior plays an important role in inflammation research [1–3]. The velocity distribution of rolling leukocytes indicates the intensity of inflammation response [4]. Tracking the movement of rolling leukocytes and thus acquiring their velocity distribution contribute to the understanding of the inflammation mechanism and to the development of drugs that treat inflammatory disease [5,6]. The de facto standard for intravital (living animal) microscopy is manual tracking of cells, where an operator manually identifies an individual cell in a sequence of recorded frames and the cell velocity is computed as the leukocyte displacement between frames divided by elapsed time [7]. This conventional manual tracking method is not only time-consuming but also subject to operator bias. Our aim is to develop an accurate and robust approach to automatically tracking rolling leukocytes in intravital image sequences.

Several approaches have been proposed to automatically track cells in image sequences. Methods proposed in the literature [8–10] were developed for tracking cells *in vitro* (in a flow chamber). Tracking leukocytes *in vivo* (in a living body) is more challenging due to moving background and image clutter [11]. Sato et al. proposed a method, in which a moving leukocyte was

* Corresponding author. Tel.: +1 734 936 9247; fax: +1 734 615 5513.
E-mail addresses: jingcui@med.umich.edu (J. Cui), nray1@cs.ualberta.ca (N. Ray), acton@virginia.edu (S.T. Acton), zl5y@virginia.edu (Z. Lin).
[1] Tel.: +1 780 492 3010; fax: +1 780 492 1071.
[2] Tel.: +1 434 982 2003; fax: +1 434 924 8818.
[3] Tel.: +1 434 924 6342; fax: +1 434 924 8818.

0895-6111/$ – see front matter © 2008 Elsevier Ltd. All rights reserved.
doi:10.1016/j.compmedimag.2008.06.004

extracted as traces in spatiotemporal images [12]. This method is only able to track leukocytes rolling near the blood vessel wall. Ray et al. proposed an active contour-based method, which located moving cells through minimizing an energy function defined on the basis of the smoothness, shape, size, sampling and gradient constraints [13]. However, given image clutter near the cell, such as strong edges of the blood vessel, the edge constraint becomes dominant in the energy function and "distracts" the contour from the intended target. A Monte Carlo tracker was developed by Cui et al., which estimated the leukocyte centroid by using a weighted sample set [14]. In comparison with the active contour tracking solution developed in [13], which incorporated the gradient vector flow (GVF) as the external force [15], the Monte Carlo tracker demonstrated more accurate and more robust tracking performance and was less affected by the strong edge of the blood vessel. Reyes-Aldasoro et al. proposed a keyhole tracking algorithm to track red blood cells [16]. First, a sequence of binary images containing segmented foreground objects were obtained by preprocessing videos, and then tracks were formed by linking the objects in contiguous frames. Finally, the links in tracks resulting from noise or joined sections that were considered to be split sections from a single track were removed by post-processing.

In our intravital microscopy image sequences, leukocytes were observed to rotate and to move in and out of the focal plane (changing scale) while interacting with endothelium (vessel wall). This observation indicates that the leukocyte movement involved is not limited to sole translation but also includes rotation and scaling. Neither of the methods described above took into account the latter two movements. Furthermore, a leukocyte appears dark if it is out of the focal plane. The image intensity of a dark leukocyte is similar to that of the background and the edge of its boundary is not always very distinctive, making a dark leukocyte difficult to be located.

In this paper, we report on an affine transformation invariance approach to tracking a single rolling leukocyte in intravital image sequences. The method is based on the affine transformation invariance property, which enables the accommodation of linear affine transformations (translation, rotation, and/or scaling) of the target, and a particle filter that overcomes the effect of image clutter. We compared the performance of this affine transformation invariance approach with the active contour tracking method [13] and the Monte Carlo tracker [14] in terms of an accuracy measure and a robustness measure. We also separately studied the ability of the affine transformation invariance approach to locate a dark target leukocyte and a bright target leukocyte.

Target tracking can be formulated as a Bayesian sequential estimation problem, in which a stochastic state transition model is built to approximate the evolution of the target state (position, velocity, shape, etc.). An observation model establishes the relationship between the target state and the measurement (acquired from the image), and the tracking problem boils down to estimating the unknown posterior density of the target state recursively over time conditioned on available observations [17]. In a dense image clutter environment, the image clutter may mimic the image intensity features of the target, making the observation density non-Gaussian [18,19]. In this case, there is no closed form analytic solution for the Bayesian sequential estimation. Hence, we must resort to numerical methods [20]. The particle filter is a technique that implements the Bayesian sequential estimation via Monte Carlo simulation [21]. It generates a set of particles (samples) to approximate the posterior density of the target state, where the posterior probability is simply the probability that the target has a particular state (position, velocity or shape, for example) given the observations (the images acquired up to, and including, the current frame in an image sequence). A particle filter stochastically explores multiple hypotheses and provides robust performance in highly dynamic environments.

In our proposed affine transformation invariance method, an energy function is defined such that locating the target boundary in subsequent frames is equivalent to minimization of the energy function. The energy function is based on the shape constraint, the edge constraint, and the constraints derived from the affine transformation invariance property. To estimate an optimal solution to minimize the energy function, a particle filter is utilized. The affine transformation invariance approach is able to accommodate linear affine transformations of the target without requiring the determination of the specific forms of transformations and the constituent parameters. This is different from traditional methods, which are transformation specific and require determination of the forms of the involved transformations and computation of the corresponding constituent parameters [22].

2. Materials and methods

2.1. Data set

Our data set included 50 intravital microscopy video sequences obtained from the Biomedical Engineering Department at the University of Virginia. In the intravital small animal experiments, leukocytes were imaged using transilluminated specimens. Video recordings were made by a charge-coupled device (CCD) camera attached to an intravital microscope, which had a water immersion objective SW25/0.6 numerical aperture modified for telescopic imaging [6]. The video frames were recorded at a spatial resolution of 640×480 pixels, where pixel-to-μm ratio was 4.94 pixels/μm horizontally and 4.68 pixels/μm vertically. The temporal resolution was 30 frames/s. Each video sequence included 91 frames. In each sequence, a single leukocyte was selected as a "target leukocyte". An operator manually identified the centroid of the target leukocyte in all frames by using a graphical user interface. The centroid was regarded as the groundtruth position of the target leukocyte in each frame and was used to evaluate the performance of the tracking method.

In intravital microscopy images, we observed that if a leukocyte is within the focal plane, the cell appears bright. Otherwise, it may appear dark with severely reduced contrast. The image intensity of a dark leukocyte is similar to that of the background and its boundary is not as distinctive as that of a bright leukocyte, which makes locating a dark leukocyte difficult. Among all 50 video sequences, there were 20 sequences in which the target leukocyte was dark and 30 sequences in which the target leuko-

cyte was bright (Here, the contrast reversal was due to imaging away from the focal plane.).

We compared the proposed affine transformation invariance approach with an active contour tracker using GVF as the external force model [13] and a Monte Carlo tracking approach [14]. Each tracking method was evaluated by using the groundtruth position as the reference. In addition to evaluate each tracking method in all 50 sequences, we also separately compared their ability to track the dark target leukocyte in 20 sequences and to track the bright target leukocyte in 30 sequences. All the tracking algorithms were executed with MATLAB 7.3 on a PC with a Pentium 4 (2.8 GHz) CPU and 1 GB of RAM.

2.2. Method

The proposed affine transformation invariance approach assumes that the centroid and the boundary of the target leukocyte in the first frame are known. In each subsequent frame, the centroid and the boundary of the target leukocyte are automatically located by minimizing an energy function, which is based on the shape constraint, the edge constraint, and the constraints derived from the affine transformation invariance property. To estimate an optimal solution that minimizes the energy function, a particle filter is employed. In our implementation, the target leukocyte boundary in the first frame was automatically segmented by using the gradient inverse coefficient of variation (GICOV) method, which was developed in [23]. GICOV was performed by using the leukocyte centroid that was manually identified by an operator as initialization, which was the only manual input required in our implementation.

2.2.1. Affine transformation invariance property

We represent the leukocyte contour by an ordered set of vertices. Each vertex can be represented as a linear combination of its neighboring two vertices. Considering all vertices, the relationship that each vertex is written as a linear combination of its neighboring two vertices can be represented by a matrix, which is called the shape matrix. The shape matrix is invariant under linear affine transformations [24]. This property is called the *affine transformation invariance property*, and provides the theoretical backbone for the affine transformation invariance approach to cell tracking.

Suppose that (x_c, y_c) is both the object centroid and the origin of the coordinate system. Let $[L_x, L_y]$ denote a set of ordered vertices representing the object contour, where $L_x = [l_{x,1}, l_{x,2}, \ldots, l_{x,n}]^T$, and $L_y = [l_{y,1}, l_{y,2}, \ldots, l_{y,n}]^T$, as shown in Fig. 1. The vertex $(l_{x,i}, l_{y,i})$, $i = 1, 2, \ldots, n$, represents coordinates of the ith vertex with respect to the object centroid, *i.e.*, $(l_{x,i} + x_c, l_{y,i} + y_c)$ represents the ith vertex in the true image coordinate system. Each vertex $(l_{y,i}, l_{y,i})$ can be written as a linear combination of its neighboring two vertices:

$$\begin{bmatrix} l_{x,i} \\ l_{y,i} \end{bmatrix} = \alpha_i \begin{bmatrix} l_{x,i_\alpha} \\ l_{y,i_\alpha} \end{bmatrix} + \beta_i \begin{bmatrix} l_{x,i_\beta} \\ l_{y,i_\beta} \end{bmatrix}, \tag{1}$$

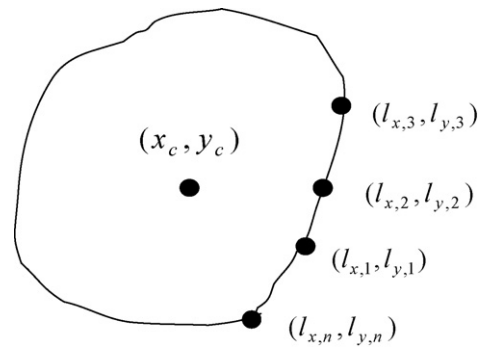

Fig. 1. The centroid and boundary points of the target.

where α_i and β_i are constant coefficients, and

$$i_\alpha = \begin{cases} i-1, & i > 1, \\ n, & i = 1, \end{cases} \qquad i_\beta = \begin{cases} i+1, & i < n, \\ 1, & i = n. \end{cases}$$

Considering all vertices and representing each vertex as a linear combination of its neighboring two vertices, we have the following relationship,

$$AL_x = 0, \tag{2}$$

$$AL_y = 0, \tag{3}$$

where

$$A = \begin{bmatrix} 1 & -\beta_1 & 0 & 0 & \ldots & -\alpha_1 \\ -\alpha_2 & 1 & -\beta_2 & 0 & \ldots & 0 \\ \vdots & \vdots & \vdots & \vdots & \ddots & \vdots \\ 0 & 0 & & -\alpha_{n-1} & 1 & -\beta_{n-1} \\ -\beta_n & 0 & \ldots & \ldots & -\alpha_n & 1 \end{bmatrix}.$$

The matrix A is called the shape matrix. Lai and Chin proved that the shape matrix is invariant under linear affine transformations [24].

The shape matrix A can be derived from the set of vertices that represents the object boundary if the latter is available. Eq. (1) can be reformulated as

$$\begin{bmatrix} l_{x,i} \\ l_{y,i} \end{bmatrix} = \begin{bmatrix} l_{x,i_\alpha} & l_{x,i_\beta} \\ l_{y,i_\alpha} & l_{y,i_\beta} \end{bmatrix} \begin{bmatrix} \alpha_i \\ \beta_i \end{bmatrix}. \tag{4}$$

If $(l_{x,i}, l_{y,i})$, $(l_{x,i_\alpha}, l_{y,i_\alpha})$ and $(l_{x,i_\beta}, l_{y,i_\beta})$ are known with $l_{x,i_\alpha} l_{y,i_\beta} \neq l_{x,i_\beta} l_{y,i_\alpha}$, α_i and β_i can be derived from

$$\begin{bmatrix} \alpha_i \\ \beta_i \end{bmatrix} = \begin{bmatrix} l_{x,i_\alpha} & l_{x,i_\beta} \\ l_{y,i_\alpha} & l_{y,i_\beta} \end{bmatrix}^{-1} \begin{bmatrix} l_{x,i} \\ l_{y,i} \end{bmatrix}. \tag{5}$$

The shape matrix A can be constructed from the values of (α_i, β_i), $i = 1, 2, \ldots, n$.

In leukocyte tracking, we assume that the centroid and the boundary of the target leukocyte in the first frame are known. That is, the set of vertices representing the leukocyte boundary is known. The shape matrix A can thus be computed by following above derivations. In the subsequent frames, even if the leukocyte translates, rotates, or scales, the shape matrix A remains

invariant. That is, the following relationship still holds:

$$AL'_x = 0, \tag{6}$$

$$AL'_y = 0, \tag{7}$$

where $[L'_x, L'_y]$ is the updated set of vertices representing the leukocyte boundary after transformations.

2.2.2. Energy function

To locate the target leukocyte, we defined an energy function, which is based on the shape constraint, the edge constraint, and the constraints derived from the affine transformation invariance property. In leukocyte tracking, we used (L_x,L_y,x_c,y_c) to denote the position of a target leukocyte in an image, where (x_c,y_c) is the centroid of the leukocyte and (L_x,L_y) denotes the set of vertices representing the leukocyte boundary with (x_c,y_c) as the origin of the coordinate system. Consequently, (L_x+x_c,L_y+y_c) represents the leukocyte boundary in the true image coordinate system, where $L_x+x_c=[l_{x,1}+x_c,l_{x,2}+x_c,\ldots,l_{x,n}+x_c]^T$ and $L_y+y_c=[l_{y,1}+y_c,l_{y,2}+y_c,\ldots,l_{y,n}+y_c]^T$. The normal directional image intensity gradient along the leukocyte boundary was defined as

$$Z(L_x+x_c, L_y+y_c) = \nabla I(L_x+x_c, L_y+y_c) \cdot N(L_x+x_c, L_y+y_c), \tag{8}$$

where $\nabla I(L_x+x_c,L_y+y_c)$ represents the image intensity gradient at (L_x+x_c,L_y+y_c) and $N(L_x+x_c,L_y+y_c)$ is the unit outward normal to the contour (L_x+x_c,L_y+y_c).

Let the position of a target leukocyte in frame t be represented by $(L_{x,t},L_{y,t},x_{c,t},y_{c,t})$. To track the leukocyte, we defined an energy function such that locating the leukocyte position in frame $t+1$ is equivalent to the minimization of the energy function:

$$\begin{aligned} E(L_x, L_y, x_c, y_c) = {} & (L_x - L_{x,t})^T(L_x - L_{x,t}) \\ & +(L_y - L_{y,t})^T(L_y - L_{y,t}) \\ & +\gamma(Z(L_x+x_c, L_y+y_c) - F)^T \\ & \times (Z(L_x+x_c, L_y+y_c) - F), \end{aligned} \tag{9}$$

subject to the constraints

$$(L_x - L_{x,t})^T A^T A(L_x - L_{x,t}) = 0, \tag{10}$$

and

$$(L_y - L_{y,t})^T A^T A(L_y - L_{y,t}) = 0, \tag{11}$$

where F is the normal directional image intensity gradient along the leukocyte boundary and γ is a constant coefficient. In our implementation, F was the normal directional image intensity gradient along the target leukocyte boundary in the first frame.

In our data set, the elapsed time between two consecutive frames was 1/30-s. In this short time period, the shape of the leukocyte was not observed to change significantly. The first two terms in Eq. (9) constrain (L_x,L_y) to remain similar to $(L_{x,t},L_{y,t})$. As the image intensity inside the leukocyte differed from that of the background, the leukocyte edge information (the image intensity gradient along the leukocyte boundary) was used as an image intensity feature to locate the leukocyte. The third term in Eq. (9) indicates that the normal directional image intensity gradient along the contour (L_x+x_c,L_y+y_c) is expected to match that along the leukocyte boundary. Eqs. (10) and (11) are derived from the affine transformation invariance property. Under linear affine transformations, in frame $t+1$, (L_x,L_y) is expected to satisfy the affine transformation invariance constraints, that is, $AL_x=0$ and $AL_y=0$. In frame t, $AL_{x,t}=0$ and $AL_{y,t}=0$. Consequently, $A(L_x-L_{x,t})=0$ and $A(L_y-L_{y,t})=0$ are obtained, from which Eqs. (10) and (11) can be derived.

Eqs. (10) and (11) can be incorporated into Eq. (9) by using the Lagrangian formulation,

$$\begin{aligned} E(L_x, L_y, x_c, y_c) = {} & \lambda(L_x - L_{x,t})^T A^T A(L_x - L_{x,t}) \\ & +\lambda(L_y - L_{y,t})^T A^T A(L_y - L_{y,t}) \\ & +(L_x - L_{x,t})^T(L_x - L_{x,t}) \\ & +(L_y - L_{y,t})^T(L_y - L_{y,t}) \\ & +\gamma(Z(L_x+x_c, L_y+y_c) - F)^T \\ & \times (Z(L_x+x_c, L_y+y_c) - F) \\ = {} & (L_x - L_{x,t})^T(\lambda A^T A + I)(L_x - L_{x,t}) \\ & +(L_y - L_{y,t})^T(\lambda A^T A + I)(L_y - L_{y,t}) \\ & +\gamma(Z(L_x+x_c, L_y+y_c) - F)^T \\ & \times (Z(L_x+x_c, L_y+y_c) - F), \end{aligned} \tag{12}$$

where λ is the Lagrangian multiplier. The energy function was based on the affine transformation invariance constraint, the target leukocyte shape constraint and the target leukocyte edge constraint. The parameters λ and γ are weight coefficients of the affine transformation invariance constraint and the edge constraint, respectively. As a result, locating the target leukocyte in frame $t+1$ can be performed by minimizing the energy function. That is,

$$(L_{x,t+1}, L_{y,t+1}, x_{c.t+1}, y_{c,t+1}) = \underset{L_x,L_y,x_c,y_c}{arg\min}\ E(L_x, L_y, x_c, y_c). \tag{13}$$

2.2.3. Estimation of the optimal solution

Since the energy function Eq. (12) is non-convex, its optimal solution cannot be written in a closed form and solved in a straightforward way. We applied a particle filter to estimate the optimal solution. In frame $t+1$, to locate the target leukocyte, we generated a sample set $\{L^{(m)}_{x,t+1}, L^{(m)}_{y,t+1}, x^{(m)}_{c,t+1}, y^{(m)}_{c,t+1}\}^M_{m=1}$, where M is the size of the sample set, in such a way that the sample with the largest weight makes the energy function minimal. The *maximum a posteriori* (MAP) estimation of the sample set was thus used as the optimal solution and the estimated target leukocyte position.

In the Bayesian sequential estimation scenario, the target state was defined as the target leukocyte posi-

tion, that is, $X_{t+1} = (L_{x,t+1}, L_{y,t+1}, x_{c,t+1}, y_{c,t+1})$. A particle filter generated a sample set to approximate the posterior density $p(L_{x,t+1}, L_{y,t+1}, x_{c,t+1}, y_{c,t+1}|Z_{1:t+1})$, where $Z_{1:t+1}$ represents the image intensity observation from frame 1 to frame $t+1$. Suppose that, in frame t, the sample set $\{L_{x,t}^{(m)}, L_{y,t}^{(m)}, x_{c,t}^{(m)}, y_{c,t}^{(m)}, \pi_t^{(m)}\}_{m=1}^{M}$ approximates the posterior density $p(L_{x,t}, L_{y,t}, x_{c,t}, y_{c,t}|Z_{1:t})$, where $\pi_t^{(m)}$ is the associated weight of the sample $(L_{x,t}^{(m)}, L_{y,t}^{(m)}, x_{c,t}^{(m)}, y_{c,t}^{(m)})$. The posterior density $p(L_{x,t+1}, L_{y,t+1}, x_{c,t+1}, y_{c,t+1}|Z_{1:t+1})$ can be expressed as

$$\begin{aligned} &p(L_{x,t+1}, L_{y,t+1}, x_{c,t+1}, y_{c,t+1}|Z_{1:t+1}) \\ &\quad \propto p(Z_{t+1}|L_{x,t+1}, L_{y,t+1}, x_{c,t+1}, y_{c,t+1}) \\ &\quad \times \sum_{m=1}^{M} p(L_{x,t+1}, L_{y,t+1}, x_{c,t+1}, y_{c,t+1}|L_{x,t} = L_{x,t}^{(m)}, \\ &\quad L_{y,t} = L_{y,t}^{(m)}, x_{c,t} = x_{c,t}^{(m)}, y_{c,t} = y_{c,t}^{(m)})\pi_t^{(m)}. \end{aligned} \tag{14}$$

Under linear affine transformations, the relationship of the target leukocyte position in two consecutive frames (frame t and frame $t+1$) can be formulated as

$$\begin{bmatrix} L_{x,t+1} \\ L_{y,t+1} \\ x_{c,t+1} \\ y_{c,t+1} \end{bmatrix} = \begin{bmatrix} \rho_{x,t+1}\cos\theta_{t+1} & -\rho_{x,t+1}\sin\theta_{t+1} & 0 & 0 \\ \rho_{y,t+1}\sin\theta_{t+1} & \rho_{y,t+1}\cos\theta_{t+1} & 0 & 0 \\ 0 & 0 & 1 & 0 \\ 0 & 0 & 0 & 1 \end{bmatrix} \times \begin{bmatrix} L_{x,t} \\ L_{y,t} \\ x_{c,t} \\ y_{c,t} \end{bmatrix} + \begin{bmatrix} 0 \\ 0 \\ \Delta x_{c,t+1} \\ \Delta y_{c,t+1} \end{bmatrix}, \tag{15}$$

where $\rho_{x,t+1}$ and $\rho_{y,t+1}$ represent the scaling coefficient along the horizontal and the vertical direction, respectively, $\Delta x_{c,t+1}$ and $\Delta y_{c,t+1}$ denote the horizontal and the vertical translation, respectively, and θ_{t+1} is the rotation angle. Because of the 1/30-s elapsed time between two consecutive frames, the rotation angle θ_{t+1} is almost zero, and $\sin\theta_{t+1} \approx 0$. The transformation in Eq. (15) can be approximated by

$$\begin{bmatrix} L_{x,t+1} \\ L_{y,t+1} \\ x_{c,t+1} \\ y_{c,t+1} \end{bmatrix} \approx \begin{bmatrix} \rho_{x,t+1}\cos\theta_{t+1} & 0 & 0 & 0 \\ 0 & \rho_{y,t+1}\cos\theta_{t+1} & 0 & 0 \\ 0 & 0 & 1 & 0 \\ 0 & 0 & 0 & 1 \end{bmatrix} \times \begin{bmatrix} L_{x,t} \\ L_{y,t} \\ x_{c,t} \\ y_{c,t} \end{bmatrix} + \begin{bmatrix} 0 \\ 0 \\ \Delta x_{c,t+1} \\ \Delta y_{c,t+1} \end{bmatrix} \tag{16}$$

We assumed that $L_{x,t+1}$ depends only on $L_{x,t}$, $L_{y,t+1}$ depends only on $L_{y,t}$, and $(x_{c,t+1}, y_{c,t+1})$ depends only on $(x_{c,t}, y_{c,t})$. Eq. (14) can thus be simplified to

$$\begin{aligned} &p(L_{x,t+1}, L_{y,t+1}, x_{c,t+1}, y_{c,t+1}|Z_{1:t+1}) \\ &\quad \propto p(Z_{t+1}|L_{x,t+1}, L_{y,t+1}, x_{c,t+1}, y_{c,t+1}) \\ &\quad \times \sum_{m=1}^{M} p(L_{x,t+1}|L_{x,t} = L_{x,t}^{(m)}) p(L_{y,t+1}|L_{y,t} = L_{y,t}^{(m)}) \\ &\quad \times p(x_{c,t+1}, y_{c,t+1}|x_{c,t} = x_{c,t}^{(m)}, y_{c,t} = y_{c,t}^{(m)})\pi_t^{(m)}. \end{aligned} \tag{17}$$

Based on the particle filter framework and Eq. (15), the sample set $\{L_{x,t+1}^{(m)}, L_{y,t+1}^{(m)}, x_{c,t+1}^{(m)}, y_{c,t+1}^{(m)}, \pi_{t+1}^{(m)}\}_{m=1}^{M}$, with $\pi_{t+1}^{(m)}$ being the associated weight, that approximates the posterior density $p(L_{x,t+1}, L_{y,t+1} x_{c,t+1}, y_{c,t+1}|Z_{1:t+1})$ was generated in the following steps:

a. Resample from the sample set $\{L_{x,t}^{(m)}, L_{y,t}^{(m)}, x_{c,t}^{(m)}, y_{c,t}^{(m)}, \pi_t^{(m)}\}_{m=1}^{M}$, i.e., draw sample $(L_{x,t+1}^{'(m)}, L_{y,t+1}^{'(m)}, x_{c,t+1}^{'(m)}, y_{c,t+1}^{'(m)}) = (L_{x,t}^{(p)}, L_{y,t}^{(p)}, x_{c,t}^{(p)}, y_{c,t}^{(p)})$ with probability $\pi_t^{(p)}$ where $p \in \{1, 2, \ldots, M\}$ and $m = 1, 2, \ldots, M$.
b. Generate a new sample $L_{x,t+1}^{(m)}$ from $p(L_{x,t+1}|L_{x,t} = L_{x,t+1}^{'(m)})$, $L_{y,t+1}^{(m)}$ from $p(L_{y,t+1}|L_{y,t} = L_{y,t+1}^{'(m)})$, and $(x_{c,t+1}^{(m)}, y_{c,t+1}^{(m)})$ from $p(x_{c,t+1}, y_{c,t+1}|x_{c,t} = x_{c,t+1}^{'(m)}, y_{c,t} = y_{c,t+1}^{'(m)})$ for $m = 1, 2, \ldots, M$.
c. Weight the new sample set $\{L_{x,t+1}^{(m)}, L_{y,t+1}^{(m)}, x_{c,t+1}^{(m)}, y_{c,t+1}^{(m)}\}_{m=1}^{M}$ by the image intensity observation.

$$\pi_{t+1}^{(m)} = \frac{p(Z_{t+1}|L_{x,t+1}=L_{x,t+1}^{(m)}, L_{y,t+1}=L_{y,t+1}^{(m)}, x_{c,t+1}=x_{c,t+1}^{(m)}, y_{c,t+1}=y_{c,t+1}^{(m)})}{\sum_{j=1}^{M} p(Z_{t+1}|L_{x,t+1}=L_{x,t+1}^{(j)}, L_{y,t+1}=L_{y,t+1}^{(j)}, x_{c,t+1}=x_{c,t+1}^{(j)}, y_{c,t+1}=y_{c,t+1}^{(j)})}, \quad m = 1, 2, \ldots, M. \tag{18}$$

State transition models $p(L_{x,t+1}|L_{x,t})$, $p(L_{y,t+1}|L_{y,t})$ and $p(x_{c,t+1}, y_{c,t+1}|x_{c,t}, y_{c,t})$ were defined to generate the sample set $\{L_{x,t+1}^{(m)}, L_{y,t+1}^{(m)}, x_{c,t+1}^{(m)}, y_{c,t+1}^{(m)}\}_{m=1}^{M}$. The first two terms in the energy function Eq. (12) constrain the shape change of the target leukocyte between two consecutive frames and enforce the affine transformation invariance property. Based on these constraints, we defined

$$p(L_{x,t+1}|L_{x,t}) \propto \exp\left(\frac{-(L_{x,t+1} - L_{x,t})^{\mathrm{T}}(\lambda A^{\mathrm{T}}A + I)(L_{x,t+1} - L_{x,t})}{2\sigma^2}\right), \tag{19}$$

$$p(L_{y,t+1}|L_{y,t}) \propto \exp\left(\frac{-(L_{y,t+1} - L_{y,t})^{\mathrm{T}}(\lambda A^{\mathrm{T}}A + I)(L_{y,t+1} - L_{y,t})}{2\sigma^2}\right), \tag{20}$$

in which $p(L_{x,t+1}|L_{x,t})$ and $p(L_{y,t+1}|L_{y,t})$ are Gaussian densities with standard deviation σ. The standard deviation denotes the range of the shape variation of the target leukocyte between two consecutive frames. The density $p(x_{c,t+1}, y_{c,t+1}|x_{c,t}, y_{c,t})$ was

defined as

$$p(x_{c,t+1}, y_{c,t+1}|x_{c,t}, y_{c,t}) \propto \exp\left(-\frac{(x_{c,t+1}-x_{c,t})^2}{2\sigma_x^2}\right) \exp\left(-\frac{(y_{c,t+1}-y_{c,t})^2}{2\sigma_y^2}\right), \quad (21)$$

where σ_x and σ_y are standard deviations of the Gaussian densities, representing the range of the leukocyte horizontal and vertical translations between two consecutive frames, respectively.

The sample $(x_{c,t+1}^{(m)}, y_{c,t+1}^{(m)})$ can be generated directly from Eq. (21). The generation of sample $(L_{x,t+1}^{(m)}, L_{y,t+1}^{(m)})$ is not trivial. Based on $p(L_{x,t+1}|L_{x,t})$ (Eq. (19)) and $p(L_{y,t+1}|L_{y,t})$ (Eq. (20)), we applied the Cholesky factorization to obtain the sample $(L_{x,t+1}^{(m)}, L_{y,t+1}^{(m)})$. Suppose that D is the Cholesky factorization of $\lambda A^{\mathrm{T}}A + I$, that is,

$$D^{\mathrm{T}}D = \lambda A^{\mathrm{T}}A + I. \quad (22)$$

Let $u_{x,t+1} = D(L_{x,t+1} - L_{x,t})$. Eqs. (19) and (20) can be written as

$$p(L_{x,t+1}|L_{x,t}) \propto \exp\left(\frac{-u_{x,t+1}^{\mathrm{T}}u_{x,t+1}}{2\sigma^2}\right), \quad (23)$$

and

$$p(L_{y,t+1}|L_{y,t}) \propto \exp\left(\frac{-u_{y,t+1}^{\mathrm{T}}u_{y,t+1}}{2\sigma^2}\right), \quad (24)$$

respectively.

The above equations imply that $u_{x,t+1}$ and $u_{y,t+1}$ are random vectors with normal distribution $N(0,\sigma^2 I_{n\times 1})$. Therefore, we first generated the samples $u_{x,t+1}^{(m)}$ and $u_{y,t+1}^{(m)}$ from the normal distribution $N(0,\sigma^2 I_{n\times 1})$ and then derived the samples $L_{x,t+1}^{(m)}$ and $L_{y,t+1}^{(m)}$ as

$$L_{x,t+1}^{(m)} = D^{-1}u_{x,t+1}^{(m)} + L_{x,t}^{(m)}, \quad (25)$$

$$L_{y,t+1}^{(m)} = D^{-1}u_{y,t+1}^{(m)} + L_{y,t}^{(m)}. \quad (26)$$

The observation model $p(Z_{t+1}|L_{x,t+1},L_{y,t+1},x_{c,t+1},y_{c,t+1})$ was defined to weight the sample set $\{L_{x,t+1}^{(m)}, L_{y,t+1}^{(m)}, x_{c,t+1}^{(m)}, y_{c,t+1}^{(m)}\}_{m=1}^{M}$. The third term in the energy function Eq. (12) constrains the normal directional image intensity gradient along the contour $(L_{x,t+1},x_{c,t+1},L_{y,t+1},y_{c,t+1})$, forcing it to match that along the target leukocyte boundary. Based on this constraint, the observation model was defined as

$$p(Z_{t+1}|L_{x,t+1}, L_{y,t+1}, x_{c,t+1}, y_{c,t+1}) \propto \exp\left(\frac{-\gamma(V_{t+1}-F)^{\mathrm{T}}(V_{t+1}-F)}{2\sigma^2}\right), \quad (27)$$

where $p(Z_{t+1}|L_{x,t+1},L_{y,t+1}x_{c,t+1},y_{c,t+1})$ is a Gaussian density with standard deviation $\sigma/\sqrt{\gamma}$, and $V_{t+1} = Z(L_{x,t+1},x_{c,t+1},L_{y,t+1},y_{c,t+1})$ (defined in Eq. (8)) represents the normal directional image intensity gradient at $(L_{x,t+1},x_{c,t+1},L_{y,t+1},y_{c,t+1})$. The standard deviation represents the range of the variation of the image intensity gradient along the contour $(L_{x,t+1},x_{c,t+1},L_{y,t+1},y_{c,t+1})$ from that along the target leukocyte boundary. Large value of γ makes the standard deviation $\sigma/\sqrt{\gamma}$ small, which indicates strong edge constraint.

Based on Eqs. (19)–(21) and (27), Eq. (14) can be written as

$$p(L_{x,t+1}, L_{y,t+1}, x_{c,t+1}, y_{c,t+1}|Z_{1:t+1}) \propto \sum_{m=1}^{M}\exp\left(\frac{-E(L_{x,t+1}, L_{y,t+1}, x_{c,t+1}, y_{c,t+1})}{2\sigma^2}\right) \exp\left(-\frac{(x_{c,t+1}-x_{c,t}^{(m)})^2}{2\sigma_x^2}\right)\exp\left(-\frac{(y_{c,t+1}-y_{c,t}^{(m)})^2}{2\sigma_y^2}\right)\pi_t^{(m)}. \quad (28)$$

Eq. (28) implies that, if the sample set $\{L_{x,t+1}^{(m)}, L_{y,t+1}^{(m)}, x_{c,t+1}^{(m)}, y_{c,t+1}^{(m)}\}_{m=1}^{M}$ has been generated, among all the samples, the sample with the largest weight $p(Z_{t+1}|L_{x,t+1}^{(m)}, L_{y,t+1}^{(m)}, x_{c,t+1}^{(m)}, y_{c,t+1}^{(m)})$ makes the energy function $E(L_{x,t+1}^{(m)}, L_{y,t+1}^{(m)}, x_{c,t+1}^{(m)}, y_{c,t+1}^{(m)})$ minimum. Therefore, the MAP estimation of the sample set $\{L_{x,t+1}^{(m)}, L_{y,t+1}^{(m)}, x_{c,t+1}^{(m)}, y_{c,t+1}^{(m)}, \pi_{t+1}^{(m)}\}_{m=1}^{M}$ was used as the estimated minimum solution for the energy function and the estimated target leukocyte position in frame $t+1$.

2.2.4. Performance measures

To evaluate the performance of the tracking method, four performance indices were considered [25]:

(1) *Percentage of frames tracked*: The leukocyte in each frame was considered as tracked if the distance between the estimated target leukocyte centroid position and the groundtruth position was less than a threshold (2 μm in our study). Dividing the number of frames tracked by the total number of frames in the image sequence, we obtained the percentage of frames tracked.

(2) *Root mean square error* (*RMSE*): The RMSE was computed by

$$\mathrm{RMSE} = \sqrt{\frac{\sum_{t=1}^{N}((\hat{x}_{c,t}-x_{c,t})^2 + (\hat{y}_{c,t}-y_{c,t})^2)}{N}}, \quad (29)$$

where $(\hat{x}_{c,t}, \hat{y}_{c,t})$ and $(x_{c,t},y_{c,t})$ are, respectively, the estimated target leukocyte centroid position and the groundtruth position in frame t, and N is the total number of frames. To better compare the accuracy of a tracking method, in each sequence, we computed the RMSE only in the frames in which the target leukocyte was tracked.

(3) *Last frame tracked*: If the last frame in the video sequence was tracked, we regarded the sequence as "last frame tracked".

(4) 100% *frames tracked*: If all the frames in the video sequence were tracked, we considered the sequence as one with "100% frames tracked".

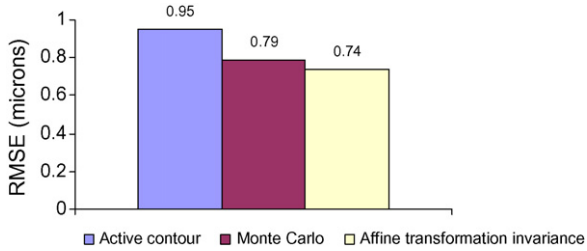

Fig. 2. RMSE with the three methods for tracking 50 sequences.

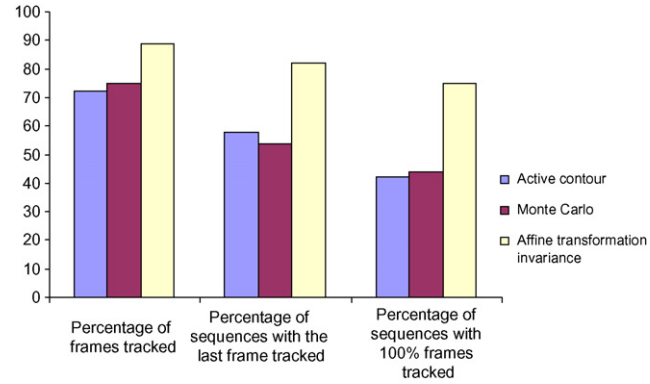

Fig. 3. Percentage of frames tracked, percentage of sequences with the last frame tracked and percentage of sequences with 100% frames tracked with the three methods for tracking 50 sequences (%).

3. Results

3.1. Leukocyte tracking within intravital microscopy image sequences

For tracking the target leukocyte in our data set of 50 intravital microscopy image sequences, the parameters of the proposed affine transformation invariance approach were set as $\lambda = 1$, $\gamma = 0.25$, $\sigma = 1$, $\sigma_x = 2$, $\sigma_y = 2$, and the sample size M was 100. Figs. 2 and 3 compare the tracking results of the active contour tracking method, the Monte Carlo tracker, and the affine transformation invariance approach. Fig. 2 shows the RMSE results where a lower RMSE indicates a higher accuracy. The RMSEs were 0.95 μm, 0.79 μm and 0.74 μm, respectively, for the active contour tracking method, the Monte Carlo tracker, and the affine transformation invariance approach. Fig. 3 and Table 1 show the percentage of frames tracked, the percentage of sequences with the last frame tracked, and the percentage of sequences with 100% (all) frames tracked, where large percentage values indicate that the tracking method is able to locate the target leukocyte in more frames and demonstrates more robust tracking performance. The percentage of frames tracked were 72%, 75% and 89% for the active contour tracking method, the Monte Carlo tracker and the affine transformation invariance approach, respectively. The percentage of sequences with the last frame tracked were 58%, 54% and 82%, and

Table 1
Percentage of frames tracked, percentage of sequences with the last frame tracked and percentage of sequences with 100% frames tracked with the three methods for tracking 50 sequences (%)

	Percentage of frames tracked (%)	Percentage of sequences with the last frame tracked (%)	Percentage of sequences with 100% frames tracked (%)
Active contour	72	58	42
Monte Carlo	75	54	44
Affine transformation invariance	89	82	75

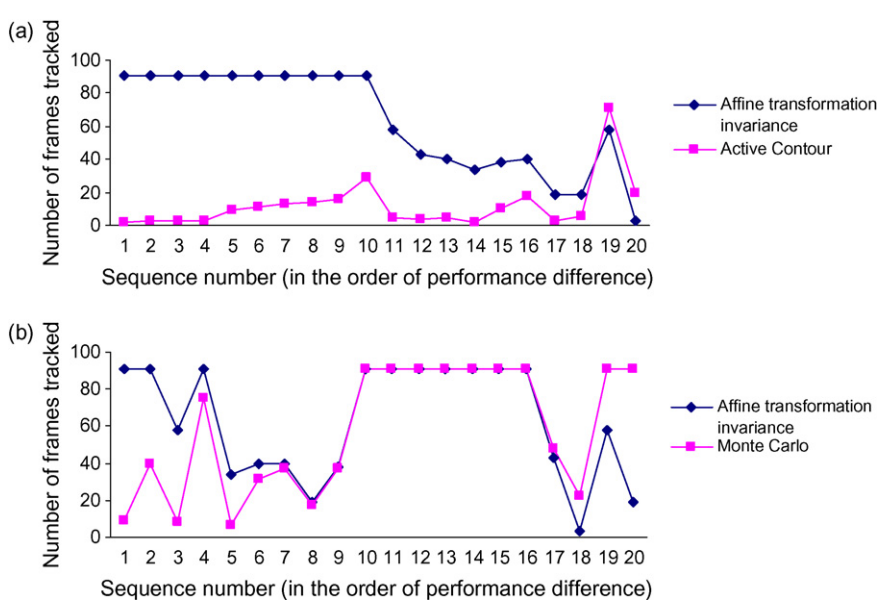

Fig. 4. Number of frames tracked in 20 sequences (dark target leukocyte).

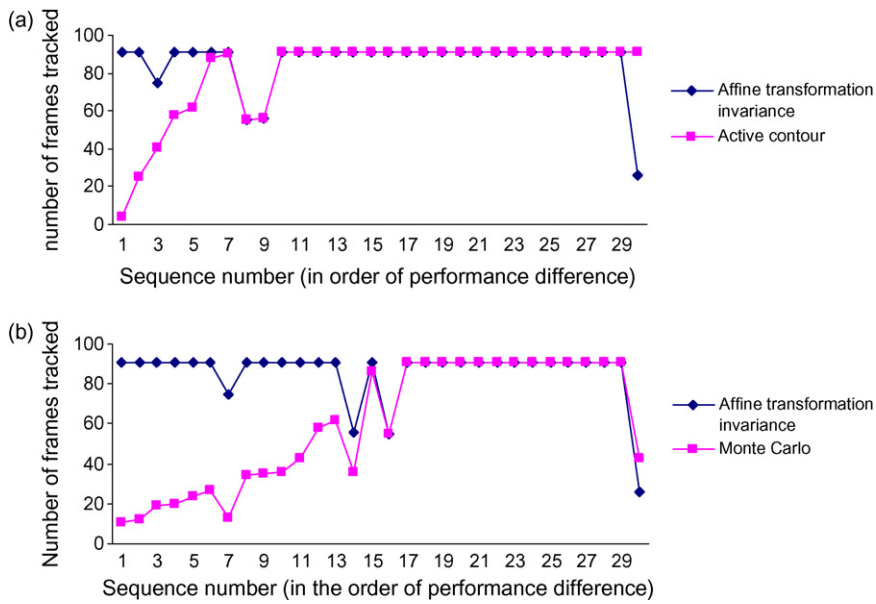

Fig. 5. Number of frames tracked in 30 sequences (bright target leukocyte).

the percentage of sequences with 100% (all) frames tracked were 42%, 44% and 75%, respectively, for the three tracking methods.

We also compared the ability of the three tracking methods to locate a dark target leukocyte and to track a bright target leukocyte. The number of frames tracked in each sequence was used as a performance measure to evaluate the tracking method. Large number of frames tracked indicates robust tracking performance as the tracking method is able to locate the target leukocyte in more frames. Fig. 4 shows the result of tracking a dark target leukocyte in 20 sequences. When compared with the active contour tracking method, the affine transformation invariance approach tracked more frames in 18 sequences and fewer frames in 2 sequences. When compared with the Monte Carlo tracker, the affine transformation invariance approach tracked more frames in 9 sequences, the same number of frames in 7 sequences and fewer frames in 4 sequences. Fig. 5 shows the result of tracking 30 sequences in which the target leukocyte was bright. The affine transformation invariance approach demonstrated superior performance in 7 sequences, equal performance in 22 sequences, and inferior performance in 1 sequence when compared with the active contour tracking method. It outperformed the Monte Carlo tracker in 15 sequences and underperformed in 1 sequence. In 14 sequences, the two methods tracked the same number of frames.

Fig. 6 shows an example of tracking a dark target leukocyte. The red contour marks the estimated target leukocyte boundary and the red '*' denotes the estimated target centroid. Fig. 6(a) and (b) show the tracking result of the active contour tracking method and the affine transformation invariance approach, respectively. As seen in Fig. 6(a), the active contour tracking method is "distracted" by the strong edge caused by the vessel wall, while the affine transformation invariance approach is able to successfully locate the target leukocyte, as shown in Fig. 6(b).

3.2. Tracking within synthetic image sequences

To illustrate that the proposed affine transformation invariance tracking approach is able to accommodate linear affine transformations, we constructed a synthetic image sequence in which the target experiences translation, rotation and scaling transformations and there exists image clutter (in the form of a strong edge and objects with similar shape as the target) in the image. The parameters were set as $\lambda = 10$, $\gamma = 2.5$, $\sigma = 5$, $\sigma_x = 2$, and $\sigma_y = 2$. The sample size M was 300. Fig. 7 shows several selected frames of the tracking result. The estimated target position is denoted by the target boundary (the red contour) and the centroid position (the red '*'). As seen in Fig. 7, the affine transformation invariance approach is able to successfully locate the target boundary although the target experiences linear affine transformations and there exists clutter in the image.

Note that the objective of this synthetic study is to examine the performance of the tracker over a range of linear affine transformations rather than to test the sensitivity to different levels of clutter. For quantification of clutter in regards to recognition and detection, please refer to the literature [26,27].

4. Discussion

In this study, we developed an affine transformation invariance approach to automatically tracking a single rolling leukocyte in intravital sequences and compared its performance with an active contour tracking method and a Monte Carlo tracker. Four performance measures were used to evaluate the tracking method. One measure (RMSE) quantifies the tracking accuracy. The other three measures relate to tracking robustness; these are the percentage of frames tracked, the percentage of sequences with the last frame tracked, and the percentage of sequences with 100% (all) frames tracked. The affine transformation invariance approach had a slightly lower RMSE than the

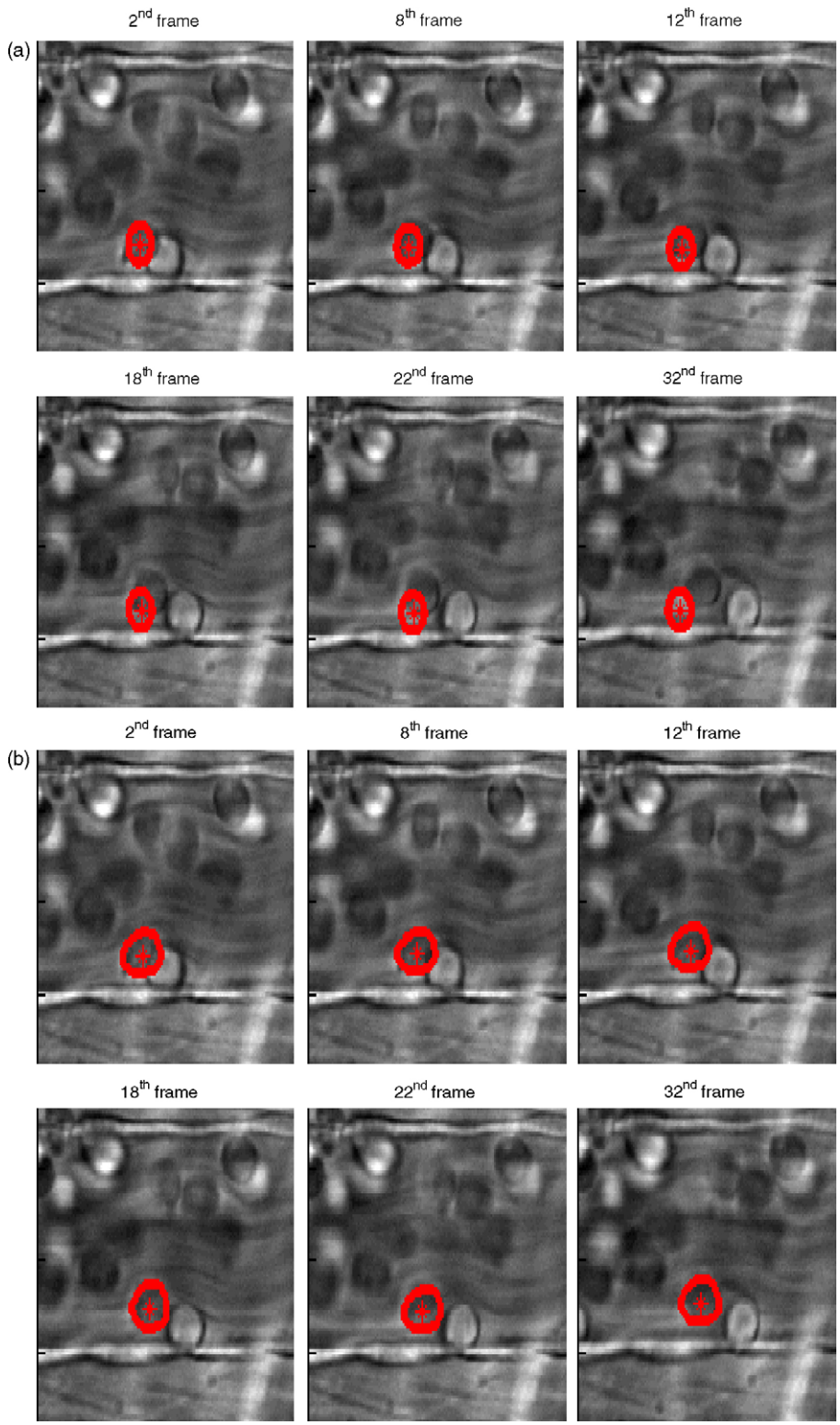

Fig. 6. Result of tracking an intravital image sequence: (a) active contour tracking method and (b) affine transformation invariance approach. (For interpretation of the references to colour in text, the reader is referred to the web version of the article.)

Monte Carlo tracker (0.74 μm vs. 0.79 μm). The RMSE of the active tracking method was much higher (0.95 μm). This indicates that the affine transformation invariance approach and the Monte Carlo tracker demonstrated more accurate performance than the active contour tracking method. The active contour tracking method and the Monte Carlo tracker demonstrated similar performance for robustness. The percentage of frames tracked, the percentage of sequences with the last frame tracked and the percentage of sequences with 100% (all) frames tracked were 72% vs. 75%, 58% vs. 54%, and 42% vs. 44%, respectively.

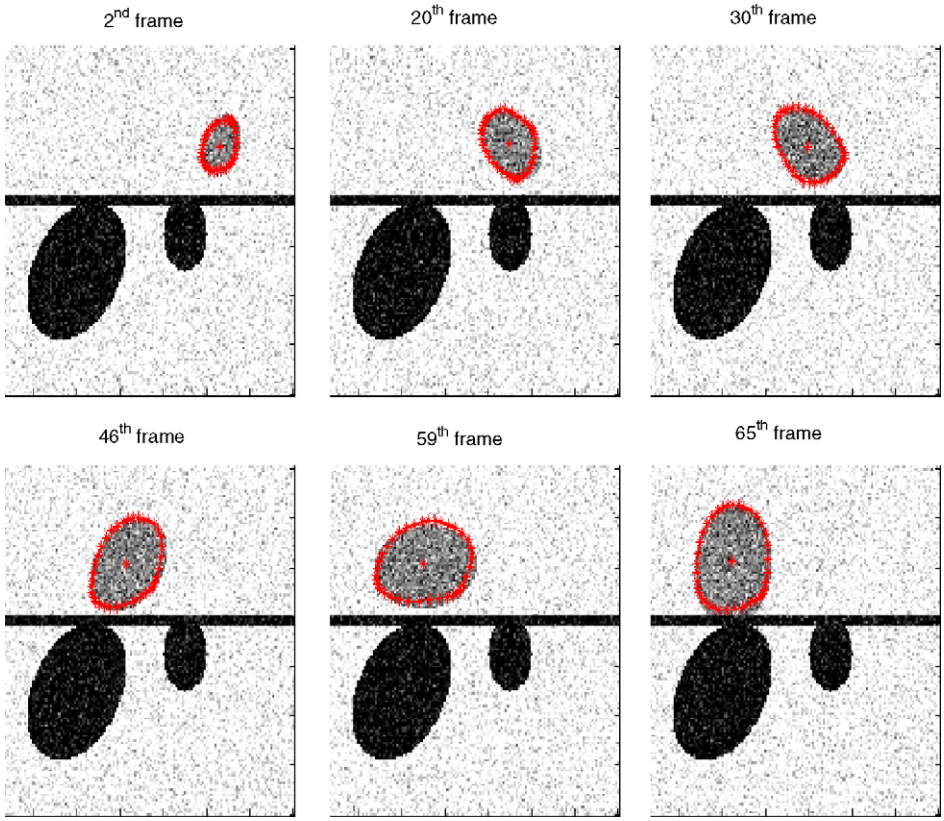

Fig. 7. The example of tracking a synthetic image sequence. (For interpretation of the references to colour in text, the reader is referred to the web version of the article.)

The corresponding results of the affine transformation invariance approach were 89%, 82% and 75%, respectively, which demonstrated a much stronger robust tracking ability. The measure "100% (all) frames tracked," which requires that in all the frames the RMSE should be less than the threshold, is more strict than the measure "the last frame tracked," which only requires that, the RMSE should be less than the threshold in the last frame. However, the measure "the last frame tracked" does provide useful information that a cell is tracked to the end of the sequence.

We also separately studied the ability of the three methods to track a dark target leukocyte and a bright target leukocyte by using the number of frames tracked as a performance measure. For tracking the dark target leukocyte in 20 sequences, the active contour tracking method showed poor performance. As shown in Fig. 4(a), in most sequences, the number of frames tracked was low, which means that the target was lost very soon. One reason for this might be that the image intensity gradient along a dark leukocyte boundary is not very distinctive and the strong edge nearby the target "distracts" the active contour tracking method. The affine transformation invariance approach performed slightly better than the Monte Carlo tracker with a larger number of frames tracked in more sequences, as shown in Fig. 4(b). As for tracking the bright target leukocyte in 30 sequences, the affine transformation invariance approach exhibited slightly better performance than the active contour tracking method, as shown in Fig. 5(a). Fig. 5(b) shows that the result of the Monte Carlo tracker was inferior to that of the affine transformation invariance approach.

The parameters of the affine transformation invariance approach can be adjusted to accommodate different tracking scenarios. In our implementation, the parameters which were set for tracking intravital sequences and the synthetic sequence were different. For tracking intravital sequences, since the leukocyte shape change between two consecutive frames was not as significant as the target in the synthetic image sequence, the parameter σ, which indicates the shape variation range of the target between two consecutive frames, was set to 1, which was lower than that set in tracking the synthetic sequence, $\sigma = 5$. The parameters of λ and γ were changed according to different σ in each parameter set. The sample sizes were also different. In tracking the synthetic sequence, more samples (sample size $M = 300$) were generated to accommodate the larger shape variation.

In some frames where the target leukocyte was occluded by other leukocytes or structures in the image, the affine transformation invariance approach failed in locating the target leukocyte. One possible reason for this might be that we used the image intensity gradient along the target leukocyte boundary in the first frame as the edge constraint. If the target leukocyte is occluded by other leukocytes or structures, the image intensity gradient information along the target leukocyte boundary changes and is different from that in the first frame. Consequently, it might not be appropriate to use the image intensity gradient information in the first frame as the edge constraint. In this case, an adaptive model might be helpful.

In examining the computational expense, the affine transformation invariance approach proves to be the most efficient of the

three methods tested. The time needed to process each frame was about 0.87 s for the active contour tracking method, 0.78 s for the Monte Carlo tracker and 0.45 s for the affine transformation invariance approach.

5. Conclusions

In this paper, based on the affine transformation invariance property and a particle filter, we proposed an affine transformation invariance approach to automatically tracking a single rolling leukocyte in intravital image sequences. Tracking experiments involving both real and synthetic data demonstrated that the proposed method was able to accommodate linear affine transformations of the target and, compared with the snake tracker and the Monte Carlo tracker, the affine transformation invariant solution exceeds the performance of the trackers tested in both accuracy and robustness.

References

[1] Kim MB, Sarelius IH. Role of shear forces and adhesion molecule distribution on P-selection-mediated leukocyte rolling in postcapillary venules. American Journal of Physiology-Heart and Circulation Physiology 2004;287:H2705–11.
[2] Xu H, Manivannan A, Goatman KA, Jiang H, Liversidge J, Sharp PF, et al. Leukocyte priming are all required for leukocyte passage across the blood–retina barrier. Journal of Leukocyte Biology 2004;75:224–32.
[3] Hafezi-Moghadam A, Thomas KL, Prorock AJ, Huo Y, Ley K. L-selectin shedding regulates leukocyte recruitment. The Journal of Experimental Medicine 2001;193(7):863–72.
[4] Jung U, Norman KE, Ramos CL, Scharffetter-Kochanek K, Beaudet AL, Ley K. Transit time of leukocytes rolling through venules controls cytokine-induced in inflammatory cell recruitment *in vivo*. Journal of Clinical Investigation 1998;102:1526–33.
[5] Kunkel EJ, Dunne JL, Ley K. Leukocyte arrest during cytokine-dependent inflammation *in vivo*. Journal of Inflammation 2000;164:3301–8.
[6] Ley K. Leukocyte recruitment as seen by intravital microscopy. In: Physiology of Inflammation. New York: Oxford University Press; 2001. p. 303–37.
[7] Hossain P, Liversidge J, Cree MJ, Manivannan A, Vieira P, Sharp PF, et al. In vivo cell tracking by scanning laser ophthalmoscopy: quantification of leukocyte kinetics. Investigative Ophthalmology & Visual Science 1998;39:1879–87.
[8] Ghosh RN, Webb WW. Automated detection and tracking of individual and clustered cell surface low density lipoprotein receptor molecules. Biophysical Journal 1994;66:1301–18.
[9] Kusumi A, Sako Y, Yamamoto M. Confined lateral diffusion of membrane receptors as studied by single particle tracking (nanovid microscopy). Effects of calcium-induced differentiation in cultured endothelial cells. Biophysical Journal 1993;65:2021–40.
[10] Zimmer C, Labruyere E, Meas-Yedid V, Guillen N, Olivo-Marin J. Segmentation and tracking of migrating cells in videomicroscopy with parametric active contours: a tool for cell-based drug testing. IEEE Transactions on Medical Imaging 2002;21:1212–21.
[11] Acton ST, Wethmar K, Ley K. Automatic tracking of leukocytes *in vivo*. Microvascular Research 2002;63:139–48.
[12] Sato Y, Chen J, Zoroofi RA, Harada N, Tamura S, Shiga T. Automatic extraction and measurement of leukocyte motion in microvessels using spatiotemporal image analysis. IEEE Transactions on Biomedical Engineering 1997;44:359–69.
[13] Ray N, Acton ST, Ley K. Tracking leukocytes in vivo with shape and size constrained active contours. IEEE Transactions on Medical Imaging 2002;21(10):1222–35.
[14] Cui J, Acton ST, Lin Z. A Monte Carlo approach to rolling leukocyte tracking *in vivo*. Medical Image Analysis 2006;10(4):598–610.
[15] Xu C, Prince JL. Snakes, shapes and gradient vector flow. IEEE Transactions on Image Processing 1998;7:359–69.
[16] Reyes-Aldasoro CC, Akerman S, Tozer GM. Measuring the velocity of fluorescently labeled red blood cells with a keyhole tracking algorithm. Journal of Microscopy 2008;229:162–73.
[17] Bar-Shalom Y, Li XR. Estimation and tracking: principles, techniques and software. Storrs, CT: YBS Publishing; 1998.
[18] Gordon N. A hybrid bootstrap filter for target tracking in clutter. IEEE Transactions on Aerospace and Electronic Systems 1997;33(1):353–8.
[19] Isard M, Blake A. Condensation—conditional density propagation for visual tracking. International Journal of Computer Vision 1998;29(1):5–28.
[20] Doucet A, Freitas N, Gordon N. Sequential Monte Carlo methods in practice. Springer; 2001.
[21] Arulampalam S, Maskell S, Gordon N, Clapp T. A tutorial on particle filters for on-line nonlinear/non-Gaussian Bayesian tracking. IEEE Transactions on Signal Processing 2002;50(2):174–89.
[22] Welser ME, Acton ST. Projection model snakes for tracking using a Monte Carlo approach. Journal of Electronic Imaging 2004;13(2):384–98.
[23] Dong G, Ray N, Acton ST. Intravital leukocyte detection using the gradient inverse coefficient of variation. IEEE Transactions on Medical Imaging 2005;24(7):910–24.
[24] Lai KF, Chin RT. Deformable contours: modeling and extraction. IEEE Transactions on Pattern Analysis and Machine Intelligence 1995;17(11):1084–90.
[25] Ray N. Tracking rolling leukocytes in vivo using active contours with motion gradient vector flow. PhD dissertation. University of Virginia; 2003.
[26] Phillips MA, Sims SRF. A signal to clutter measure for ATR performance comparison. In: Proceedings of SPIE on Automatic Target Recognition VII, vol. 3069. 1997. p. 74–81.
[27] Yu Y, Acton ST, Thornton K. Detection of radioactive seeds in ultrasound images of the prostate. In: Proceedings of IEEE International Conference on Image Processing. 2001. p. 319–22.

Jing Cui received her B.S. degree in Automatic Control from Xiamen University, Xiamen, China, in 1998, M.S. in Control Theory and Control Engineering from Chinese Academy of Space Technology, Beijing, China, in 2001, Ph.D. in Electrical Engineering from University of Virginia, Charlottesville, Virginia, in 2006. She is currently a research fellow in the Department of Radiology at the University of Michigan, Ann Arbor, Michigan. Her research interests include computer-aided diagnosis, pattern recognition, image processing, and video tracking.

Nilanjan Ray received his Bachelor degree in Mechanical Engineering from Jadavpur University, Calcutta, India, in 1995, Master's degree in Computer Science from the Indian Statistical Institute, Calcutta, in 1997, and Ph.D. in Electrical Engineering from the University of Virginia, Charlottesville, in May 2003. Nilanjan has worked as a postdoctoral fellow at Electrical and Computer Engineering Department, University of Virginia under Prof. Scott Acton's supervision. He has worked in Utopia Compression Corporation, a high-tech image/video analysis based company in Los Angeles for a year. He joined the Department of Computing Science, University of Alberta in July 2006. Nilanjan is a recipient of the CIMPA-UNESCO fellowship for image processing in 1999; the graduate fellowship at Indian Statistical Institute from 1995 to 1997; and the best student paper award from IBM Picture Processing Society presented at the IEEE International Conference on Image Processing, Rochester, NY, 2002. Nilanjan's research area is image analysis and computer vision.

Scott Acton received the M.S. degree in Electrical and Computer Engineering and the Ph.D. degree in Electrical and Computer Engineering from the University of Texas at Austin in 1990 and 1993, respectively. He has a B.S. degree in Electrical Engineering from Virginia Tech (1988). He has worked in industry for AT&T, the MITRE Corporation and Motorola, Inc. and in academia for Oklahoma State University. For his research in video tracking, Dr. Acton was given an ARO Young Investigator Award. He received the Halliburton Outstanding Young Faculty Award in 1998. In 1997, he was named the Eta Kappa Nu Outstanding Young Electrical Engineer—a national award that has been given annually since 1936. At UVa, he received the New Faculty Teaching award in

2002, was named Faculty Fellow in 2003, and became a professor in 2005. Dr. Acton is a senior member of the IEEE and has served as associate editor for the IEEE Transactions on Image Processing and the IEEE Signal Processing Letters.

Zongli Lin received his B.S. degree in Mathematics and Computer Science from Xiamen University, Xiamen, China, in 1983, his Master of Engineering degree in Automatic Control from Chinese Academy of Space Technology, Beijing, China, in 1989, and his Ph.D. degree in Electrical and Computer Engineering from Washington State University, Pullman, Washington, in May 1994. From July 1983 to July 1986, Dr. Lin worked as a control engineer at Chinese Academy of Space Technology. In January 1994, he joined the Department of Applied Mathematics and Statistics, State University of New York at Stony Brook as a visiting assistant professor, where he became an assistant professor in September 1994. Since July 1997, he has been with the Department of Electrical and Computer Engineering at University of Virginia, where he is currently a professor.